JGR Solid Earth

RESEARCH ARTICLE
10.1029/2023JB027245

Bridging the Gap Between Experimental and Natural Fabrics: Modeling Ice Stream Fabric Evolution and its Comparison With Ice-Core Data

Daniel H. Richards[1,2], Samuel S. Pegler[2], Sandra Piazolo[3], Nicolas Stoll[4,5], and Ilka Weikusat[5,6]

[1]The Australian Centre for Excellence in Antarctic Science, University of Tasmania, Hobart, Australia, [2]School of Mathematics, University of Leeds, Leeds, UK, [3]School of Earth and Environment, University of Leeds, Leeds, UK, [4]Department of Environmental Sciences, Informatics and Statistics, Ca'Foscari University Venice, Venice, Italy, [5]Alfred Wegener Institute Helmholtz Centre for Polar and Marine Research, Bremerhaven, Germany, [6]Department of Geosciences, Eberhard Karls University, Tübingen, Germany

Key Points:

- We combine an experimentally validated fabric model with satellite velocity data to compare directly to ice cores from an ice stream
- The experimentally validated model predicts the observed fabric patterns and orientations along the ice core to first-order approximation
- However, the natural fabrics produced at lower strain rates are significantly stronger than those produced in laboratory experiments

Correspondence to:
D. H. Richards,
daniel.richards@utas.edu.au

Citation:
Richards, D. H., Pegler, S. S., Piazolo, S., Stoll, N., & Weikusat, I. (2023). Bridging the gap between experimental and natural fabrics: Modeling ice stream fabric evolution and its comparison with ice-core data. *Journal of Geophysical Research: Solid Earth*, *128*, e2023JB027245. https://doi.org/10.1029/2023JB027245

Received 9 JUN 2023
Accepted 6 NOV 2023

Author Contributions:
Conceptualization: Daniel H. Richards, Samuel S. Pegler, Sandra Piazolo
Data curation: Nicolas Stoll, Ilka Weikusat
Formal analysis: Daniel H. Richards
Investigation: Daniel H. Richards
Methodology: Daniel H. Richards, Samuel S. Pegler, Sandra Piazolo
Project Administration: Ilka Weikusat
Software: Daniel H. Richards
Supervision: Samuel S. Pegler, Sandra Piazolo
Visualization: Daniel H. Richards
Writing – original draft: Daniel H. Richards
Writing – review & editing: Samuel S. Pegler, Sandra Piazolo, Nicolas Stoll

Abstract Fabrics, also known as textures or crystallographic preferred orientations, reveal information about the deformation history of the flow of polycrystalline materials, including glacial ice, olivine in the mantle, and feldspar and quartz in the crust. Ice fabrics can have an order-of-magnitude effect on the ease of flow in ice sheets. However, due to the choice of ice core drill site locations, the outputs of fabric models have mostly been compared to observations from the least dynamic regions of the ice sheet (ice divides). Recently, fabric data from an active ice stream have become available from ice cores drilled at the East Greenland Ice-core Project (EGRIP). In this work, we present a novel approach that combines satellite-derived velocity data with the fabric evolution model SpecCAF, a continuum model based on dominant dislocation creep. We directly compare model output to ice-core observations from EGRIP, allowing us to examine the quantitative predictions of calibrated fabric models alongside those of active ice streams for the first time. As the model is calibrated against laboratory experiments, it provides a surrogate to compare the evolution of fabrics under laboratory and natural conditions. The predictions show good qualitative agreement with the observed fabric patterns and orientations, suggesting that a fabric between a girdle and horizontal maximum, orientated perpendicular to the flow direction, is the characteristic ice stream fabric. A discrepancy in fabric strength is attributed to the lower strain rates of ice sheets compared to laboratory experiments, revealing a significant strain-rate dependence in the processes controlling fabric evolution.

Plain Language Summary Most materials that comprise the solid Earth, including the ice sheets and the mantle, flow viscously over long timescales. A key control of this flow is the average orientation of the crystals which make up these materials. In ice, measurements of this average orientation have to date been limited to areas where the ice deforms very slowly. Recently, data from an ice stream—a fast-flowing region in the ice sheet—have become available. In this work, we predict the alignment of ice crystals in an ice stream, using a model previously tested and validated in the laboratory. Since the model gives good predictions of the crystal alignment seen in the laboratory, it can be used to compare between laboratory results and ice sheets for the first time. We predict that the alignment of ice crystals form a pattern that is consistent with what is measured. However, the strength of the alignment is greater in ice sheets, which deform much slower than laboratory experiments.

1. Introduction

Understanding the dynamics of polycrystalline materials is fundamental to our understanding of the deformation behavior of different layers existing in planetary bodies. These polycrystalline materials include olivine in the Earth's mantle; feldspar and quartz in the crust (e.g., Behrmann & Mainprice, 1987); and glacial ice, whose dynamics are likely to control sea-level rise over the next decades and centuries (e.g., Shepherd et al., 2018). Fabrics, also called textures or Crystallographic Preferred Orientations (CPOs), represent the collective distribution of crystal orientations within a region and dictate the mechanical properties. In ice, fabrics can cause flow rates to vary by an order of magnitude in different directions (Pimienta & Duval, 1987). Yet most ice-sheet models do not include the evolution of ice fabrics. Additionally, there remain a number of key open questions

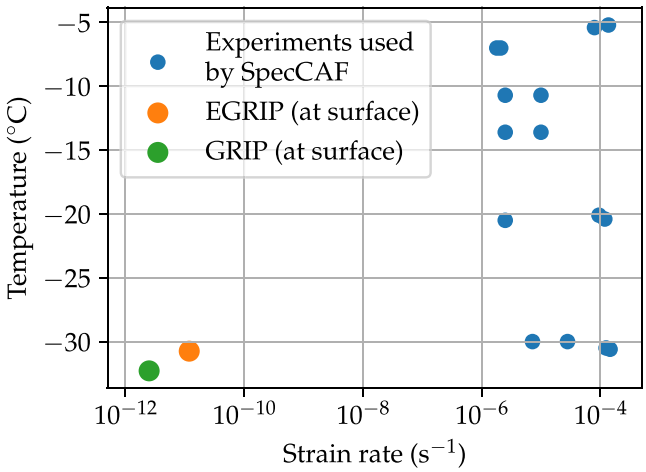

Figure 1. Strain-rate-temperature plot showing differences, primarily in strain rate, between the experiments (Craw et al., 2018; Piazolo et al., 2013; Qi et al., 2019) used to constrain SpecCAF (Richards et al., 2021), and the surface deformations at East Greenland Ice-core Project (EGRIP) (an ice stream) and Greenland Ice-core Project (GRIP) (an ice divide).

regarding the dominant deformation and recrystallization processes in ice sheets and how these processes create fabrics.

Within crystalline masses, localization of strain is common (e.g., Ramsay, 1980). However, the mechanisms underlying this localization remain enigmatic in many cases. In ice, localization is seen in ice streams: regions characterized by high-speed flow primarily resulting from sliding at the ice sheet's base. Ice streams create a dominant control of the large-scale flow of the ice sheet, being responsible for the majority of mass loss from ice sheets (e.g., Bennett, 2003). Recently, ice stream fabric data have been obtained from ice-core drilling expeditions (Stoll et al., 2021; Westhoff et al., 2021) and radar techniques (Lutz et al., 2020; Smith et al., 2017; Treverrow et al., 2010; Zeising et al., 2023). These studies have revealed a range of patterns in the fabric of the ice, generally showing grains having orientations in the plane perpendicular to the flow direction (to be reviewed in Section 2.3). It remains an open question whether our current modeling and understanding of fabric evolution can predict these naturally occurring fabric patterns which develop under strain rates that are inaccessible in the laboratory.

Ice streams contain the highest deformation rates in the Greenland Ice Sheet at around 10^{-11}–10^{-9} s^{-1}, compared to the ice sheet as a whole, where deformation rates lie in the range 10^{-15}–10^{-9} s^{-1}. Yet, due to time constraints, experiments are deformed at faster rates in the range of 10^{-7}–10^{-4} s^{-1}. There is therefore a large disparity between strain rates of deformations which form natural ice fabrics and those produced in experiments (Figure 1). It remains a key open question whether fabrics produced across these ranges in strain rates are the same, and whether the various processes that affect the fabric have significant strain-rate dependence.

In this contribution, we present the first predictions of the development of ice fabrics within an ice stream compared directly alongside ice-core observations. Our analysis employs the SpecCAF fabric evolution model (Richards et al., 2021). The model is based on the assumption that dislocation creep dominates in ice (see Section 2.1) and is directly constrained against laboratory experiments, being the only model demonstrated to predict the details of fabrics observed in these conditions. As the model is constrained at strain rates around six orders of magnitude faster than is typical in ice sheets, we are able to establish the quantitative effects of strain-rate dependence in fabric evolution between experimental and natural conditions. This has implications not only for ice, but also for olivine fabrics in the mantle, where fabric models are often constrained against experiments at much higher strain rates (e.g., Hansen et al., 2016).

To begin, we compare predictions against the simple case of an ice divide, where the deformation is unconfined compression. We then use satellite-derived surface velocity data combined with SpecCAF to predict the fabric evolution within an active ice stream. The analysis uses velocity data to determine the (Lagrangian) evolution of fabrics originating from the surface of the ice sheet through to the position of a recently extracted ice core in an ice stream, from the East Greenland Ice-Core Project (EGRIP) (Stoll et al., 2021), accounting for its changing deformation history. We compare the model predictions directly against the observational data from the ice core. The predictions provide us with a surrogate to compare fabrics produced under experimental conditions with those formed in ice sheets. The method thereby allows us to address the key question of how fabrics formed under experimental conditions differ from those in ice sheets.

2. Background

2.1. Processes Affecting Ice Fabric Evolution

Ice sheets deform under their own weight through plastic deformation, which can be described as "flow" at large scales. There is ongoing debate about the dominant mechanisms that facilitate this deformation. The most widely accepted explanation is dislocation creep (e.g., Paterson, 1999). Dislocations are line defects in the crystal lattice caused by impurities or a local excess or deficiency of hydrogen atoms (Glen, 1968). Stress on the ice lattice generates dislocations, which store energy within the ice volume. As differential stress is applied, dislocations move through the crystalline structure, causing ice deformation.

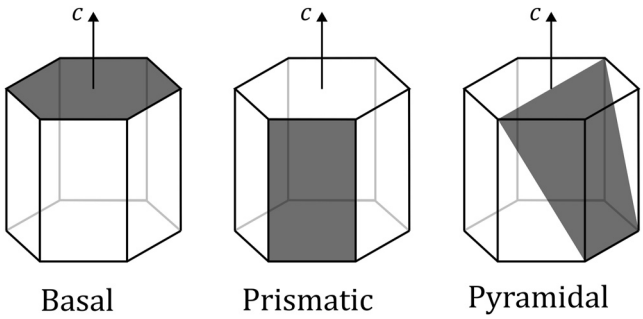

Figure 2. The figure illustrates the hexagonal crystal structure and the different slip planes along which dislocations move. The *c* axis, normal to the basal plane, is also illustrated. Basal-slip deformation is approximately 70 times easier than prismatic slip and 180 times easier than pyramidal slip (Duval et al., 1983).

Dislocations move along certain slip systems (Figure 2), with basal-slip deformation dominating due to its lower activation energy in ice. Basal-slip deformation is approximately 70 times easier than prismatic slip and 180 times easier than pyramidal slip (Duval et al., 1983). The collective orientation of basal planes, represented by the *c* axis unit normal, controls mechanical properties, leading to significant anisotropy and variations in deformation ease by an order of magnitude (Pimienta & Duval, 1987). The collective distribution of orientations is called the *fabric*.

In addition to basal-slip deformation, recrystallization processes driven by dislocation movement contribute to ice fabric formation. Migration recrystallization occurs when the difference in dislocation density across a grain boundary and, consequently, the difference in stored energy, causes the less strained grain to grow at the expense of the more strained grain (e.g., Humphreys & Hatherly, 2004). Grains favorably oriented for basal-slip deformation will accumulate fewer dislocations than other orientations, leading to growth of these grains.

Rotational recrystallization involves dislocation recovery into subgrain boundaries. These subgrains gradually rotate away from the orientation of their parent grain, forming new grains as the ice deforms (Drury et al., 1985). Since dislocations are often concentrated near grain boundaries due to stress heterogeneities (Piazolo et al., 2015), new grains are more likely to form close to these boundaries (Piazolo et al., 2008). This process results in a more dispersed orientation of new grains relative to the original grain orientation, which can be modeled as a diffusion of the orientation of *c*-axis concentrations in the orientation space (Gödert, 2003). It is currently an open question how this process varies with strain rate.

Grain boundary sliding, another deformation mechanism, involves individual grains sliding relative to each other to accommodate shape changes under differential stresses, facilitated by diffusion or dislocation glide (Goldsby & Kohlstedt, 2001). The large-scale dynamics of grain boundary sliding depends on the microscale deformation mechanism. The rheological flow law for grain boundary sliding (accommodated by diffusion) has a near-linear relationship between stress and strain rate (Coble, 1963; Herring, 1950), while the commonly adopted exponent for dislocation creep is ≈3 (Glen, 1968). Grain boundary sliding alone generates little to no fabric (e.g., Jiang et al., 2000; Svahnberg & Piazolo, 2010; Warren & Hirth, 2006). It has been suggested that grain boundary sliding may be either the dominant or a significant mechanism for the stress scales and strain-rates of ice sheets (Goldsby & Kohlstedt, 2001). However, this is controversial, as strong fabrics are typically observed in cores taken from ice sheets (Duval & Montagnat, 2002). It remains an open question whether grain boundary sliding is an important mechanism in facilitating deformation in ice sheets.

2.2. Fabric Evolution Models

Like the modeling of many physical processes, the modeling of fabric evolution necessitates a trade off between resolving fine-scale details and computational cost. Models exist that resolve interactions between grains (e.g., Castelnau, Duval, et al., 1996; Piazolo et al., 2010). These kinds of models give excellent insight into microstructural processes and have been applied to limited locations in ice sheets, such as a divide (Montagnat et al., 2012) and for a synthetic ice stream (Llorens et al., 2022). However, these models are too computationally expensive to run across multiple locations in an ice sheet.

Broadly speaking, there are two physical approaches to modeling ice fabrics without resolving grain interactions explicitly. The first is to work with grain dynamics but assume all grains experience either the same stress or strain rate (or a linear combination of the two) so that interactions between grains (and hence the smallest length scales) do not need to be resolved. The fabric evolution model that is used in Elmer/Ice falls into this category (Gagliardini et al., 2013). This model attempts to incorporate the affect of stress on the fabric, but only the recent work of Rathmann and Lilien (2021) includes the effect of recrystallization.

The second physical approach is to consider a continuum theory, motivated by the success of considering a fluid as a continuum rather than as a collection of particles. Here, a polycrystalline material is considered as a "mixture of orientations," and conservation equations for mass, momentum, energy, etc. are considered for both physical

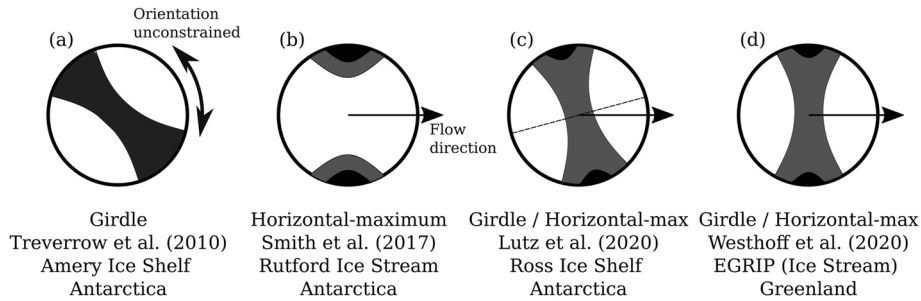

Figure 3. Schematic pole figures showing fabric data obtained from observational studies of ice streams and ice shelves. Shading represents the concentration of *c* axis orientations in that direction.

and orientation space (Faria, 2006a). For example, the fabric evolution equation from Faria (2006b) and Placidi et al. (2010) is derived by considering how grain mass is conserved over the space of possible orientations. It should be noted that although these two approaches to deriving equations are quite different the resulting equations are the same with the exception of a few terms.

SpecCAF falls into the second category, and is based on Faria (2006b) and Placidi et al. (2010). Uniquely, this fabric evolution model has been constrained against laboratory experiments, and yields excellent predictions at these strain rates of around 10^{-5} s^{-1} (Figure 1) (Richards et al., 2021).

2.3. Fabrics Observed in Ice Sheets

Historically, ice cores have been drilled at or near ice divides (a stagnation point in the ice-sheet flow), as the minimal deformation in these locations yields the most accurate, undisturbed palaeoclimate data (e.g., Dansgaard et al., 1969; Gow, 1961; Thorsteinsson et al., 1997). There is a large amount of fabric data available from these locations yet this is unrepresentative of the ice sheet as a whole. In contrast, the more limited data from fast-flowing locations are better suited for analyzing flow processes and fabric dynamics in ice sheets.

Ice streams are corridors of dynamic ice within ice sheets that flow faster than surrounding ice due to sliding at the ice-bedrock interface. Ice shelves are similarly fast-flowing regions, owing to effectively zero basal drag along the ice-ocean interface. In both regimes, the dominant deformation is often extension in the flow direction due to acceleration along streamlines.

In extension, the fabric expected by considering lattice rotation is a girdle pattern perpendicular to the flow direction (e.g., Paterson, 1999). Figure 3 presents an overview of the ice fabrics measured from ice streams and shelves. Treverrow et al. (2010) examined the fabric from drilled ice cores in the Amery Ice Shelf (Figure 3a) and observed the expected girdle fabric. It should be noted that the orientations of the measured pole figures are unconstrained because ice cores are free to rotate when drilled. In particular, the information of the orientation of the girdle relative to the flow direction is normally lost unless attempts are made to reconstruct the core's original rotation (e.g., Westhoff et al., 2021).

Recently, fabric data have become available from ice streams and ice shelves that do not exhibit the classical girdle fabric expected from unconfined extension. Smith et al. (2017) estimate that the fabric best fitting seismic data from the Rutford Ice Stream is a diffuse horizontal-maximum pattern, characterized by a cluster perpendicular to the flow direction (Figure 3b). Smith et al. (2017) attribute this pattern to compression in the cross-streamline direction at this location. Lutz et al. (2020) use a similar observational method to estimate the fabric for the Ross Ice Shelf and find that a combination of a girdle and horizontal-maximum best fits the seismic data (Figure 3c). However, in contrast to the observations of Smith et al. (2017), the clusters are not aligned perpendicular to the flow direction. Lutz et al. (2020) therefore suggest that the observed fabric is formed due to deformation by simple shear, with the shear plane perpendicular to the cross-flow direction. Recently, a deep ice core has been drilled at the EGRIP site, inside an active ice stream. This has been combined with work which constrains the orientation of drilled ice cores (Westhoff et al., 2021). The work reveals a fabric below 500 m that lies intermediate to a girdle and horizontal-maximum pattern, orientated perpendicular to the flow direction (Figure 3d).

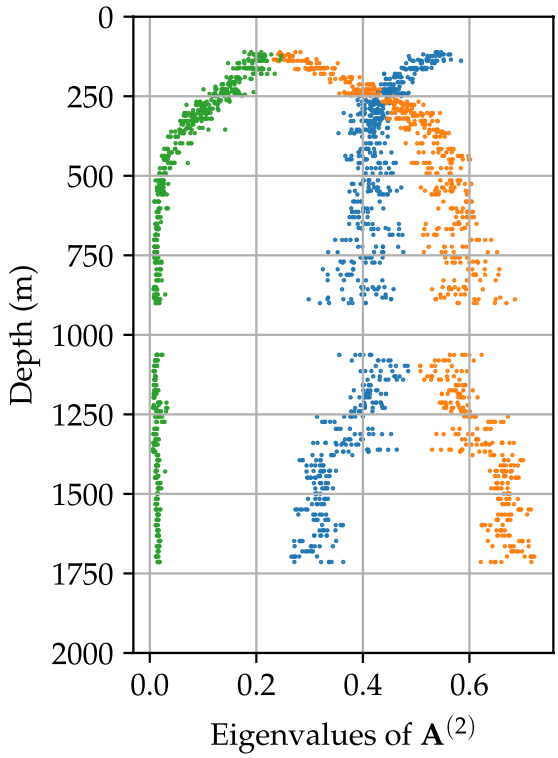

Figure 4. Figure showing the eigenvalues of the second-order orientation tensor calculated from ice cores, with depth into the East Greenland Ice-core Project (EGRIP) drill site.

2.4. Modeling of Ice-Sheet Fabrics

Historically, ice fabric evolution models have been applied to simulate fabrics at ice divides (e.g., Castelnau, Thorsteinsson, et al., 1996; Montagnat et al., 2012), with the VPSC model of Montagnat et al. (2012) giving predictions which agree with ice-core observations. It is only recently, with the availability of fabric data from the EGRIP project and from seismics, that fabric evolution models have been applied to ice streams. Lilien et al. (2021) and Llorens et al. (2022) have used a modeled velocity field to predict fabrics formed in ice streams. Generally, the modeling agrees qualitatively with observations in a broad sense, predicting a girdle perpendicular to the flow at ice stream onset, or a horizontal maximum if horizontal shear is present. However, these studies do not directly compare modeling with observations from ice cores.

Prior studies have also investigated how quickly fabrics respond to changes in deformation. In particular, Lilien et al. (2021) have tried to answer this question in order to inform large-scale approximations (e.g., Graham et al., 2018). They find fabrics respond to changes in deformation over timescales of 1,000 to 10,000 years.

Of the fabric evolution models for ice, the SpecCAF model is the only one which has been validated against laboratory experiments (Richards et al., 2021), reproducing the details of observed fabrics in experiments to excellent approximation. Therefore, it can be used as a surrogate for comparing fabrics from ice streams to those from experiments, which are deformed at much higher strain rates (Figure 1). This provides an inroad to yield new insights into ice stream dynamics and ice microstructure.

3. Data and Methods

3.1. Observed Fabric at EGRIP

For our analysis, we introduce here measured fabric data from the upper 1,714 m of the EGRIP ice core (Figure 4); data from the brittle zone at a depth of ≈1,000 m is excluded. Every ∼15 m of depth, a 55 cm long ice-core piece was cut into six samples with typical dimensions of 90 × 70 × 0.3 mm. A total of 744 samples (oriented along the ice-core axis) were analyzed directly in the EGRIP trench at −18°C. Measurements of c axis orientation were conducted to a 20 μm resolution using an automated fabric analyzer from Russel-Head Instruments (FA G50) (Wilson et al., 2003). Data were background corrected, and the CPO derived from digital image processing.

Figure 4 shows the variation in the eigenvalues of the second-order orientation tensor $\mathbf{A}$ at EGRIP with depth. When calculating $\mathbf{A}$ from grain samples, the orientation tensor is defined as a weighted sum over the grain angles:

$$A_{ij} = \sum_{g=1}^{N} w^g c_i^g c_j^g \tag{1}$$

where w^g is the weight (i.e., the estimated volume), and $\boldsymbol{c}^g$ is the measured c axis orientation of grain g. We observe a relatively fast transition from a weak fabric near the surface to eigenvalues of approximately 0.7, 0.3, 0 below 600 m. The data show small-scale oscillatory variations with depth in the intermediate and largest eigenvalues below 550 m. Analysis of the grain orientations from the ice core (Stoll et al., 2021) show that the grains are orientated to produce a girdle fabric below 350 m, which intensifies in strength down to the last glacial at 1,300 m. Below this depth, a girdle/horizontal-maximum fabric was observed.

3.2. Fabric Evolution Model: Equations and Assumptions

To model the fabric, we employ the SpecCAF model (Richards et al., 2021), which provides a fully constrained continuum model for the fabric evolution, based on a mathematical framework of Placidi et al. (2010), that is constrained using laboratory data. The fabric is described by the orientation mass density $\rho^*(\boldsymbol{x}, \boldsymbol{n}, t)$, representing the mass fraction of crystallites with c axes orientation toward orientation angle $\boldsymbol{n}$ near a region of ice at position $\boldsymbol{x}$. We work with SpecCAF in dimensional form, with governing equation

$$\frac{D\rho^*}{Dt} + \rho^* \nabla \cdot \boldsymbol{u} = -\nabla^* \cdot \left[\rho^* \boldsymbol{v}^*\right] + \lambda \nabla^{*2}(\rho^*) + \beta(\mathcal{D}^* - \langle \mathcal{D}^* \rangle)\rho^* \tag{2}$$

where ∇ is the gradient operator over position space, ∇^* is the gradient over orientation space, and $D/Dt = \partial/\partial t + \boldsymbol{u} \cdot \nabla$ is the material derivative. Inside the term $-\nabla^* \cdot [\rho^* \boldsymbol{v}^*]$, where

$$v_i^* = W_{ij} n_j - \iota(D_{ij} n_j - n_i n_j n_k D_{jk}) \tag{3}$$

is the orientation transition rate. For an individual grain, v_i^* describes how deformation due to basal-slip rotates the grain's c-axis. However, in our continuum model, this term represents the transition of mass from a certain orientation to a neighboring orientation on the unit sphere (Placidi et al., 2010). The parameter ι controls the magnitude of the effect of basal-slip deformation on the fabric. The tensors $\mathbf{D}$ and $\mathbf{W}$ represent the symmetric and antisymmetric parts of the velocity gradient tensor. The term $\lambda \nabla^{*2}(\rho^*)$ represents the effect of rotational recrystallization, where λ is a parameter controlling the magnitude of the effect. The term $\beta(\mathcal{D}^* - \langle \mathcal{D}^* \rangle)\rho^*$, where

$$\mathcal{D}^* = 5 \frac{(D_{ij} n_j)(D_{ik} n_k) - (D_{ij} n_j n_i)^2}{D_{mn} D_{nm}} \tag{4}$$

and

$$\langle \mathcal{D}^* \rangle = \int_{S^2} \frac{\rho^*}{\rho} \mathcal{D}^* \, \mathrm{d}\boldsymbol{n} \tag{5}$$

represents the effect of migration recrystallization on the fabric (forming an orientationally dependent source term). The parameter β controls the magnitude of the effect. More details and explanation of the terms in the equations, alongside discussion of the model assumptions can be found in Placidi et al. (2010) and Richards et al. (2021, 2022).

Within the context of the continuum theory, the orientation tensor (defined in a discrete sense in Equation 1) is given by

$$A_{ij} = \langle n_i n_j \rangle = \int_{S^2} \frac{\rho^*}{\rho} n_i n_j \, \mathrm{d}\boldsymbol{n} \tag{6}$$

We use the same values for the nondimensional parameters as determined in Richards et al. (2021, 2022), $\tilde{\lambda}$ and $\tilde{\beta}$, which were normalized by the strain rate $\dot{\gamma} = \sqrt{D_{ij} D_{ij}/2}$. The dimensional forms of these parameters are

$$\lambda = \tilde{\lambda}(T)\dot{\gamma}, \quad \beta = \tilde{\beta}(T)\dot{\gamma} \tag{7}$$

With the functions $\tilde{\lambda}(T)$ and $\tilde{\beta}(T)$ determined via regression against experiments, SpecCAF has been shown to give accurate predictions for fabrics produced in laboratory conditions ($\dot{\gamma} \sim 10^{-5}$ s^{-1}). Thus, by applying the model and parameters to an ice stream, we are able to generate comparisons between fabrics produced under laboratory and ice-sheet conditions. This equation is solved using spherical harmonics as in Richards et al. (2021, 2022), however here we use the Specfab numerical solver (Rathmann & Lilien, 2021; Rathmann et al., 2021).

3.3. Estimating the Deformation of an Ice Divide

As a preliminary test case, we compare SpecCAF's predictions at an ice divide with GRIP fabric data (Thorsteinsson et al., 1997). For this, a simple model is used, like in Castelnau, Thorsteinsson, et al. (1996) and Montagnat et al. (2012), though our method differs slightly. It is assumed the core is drilled at a perfect ice divide, such that it only experiences unconfined compression. The vertical shear rate is assumed to follow

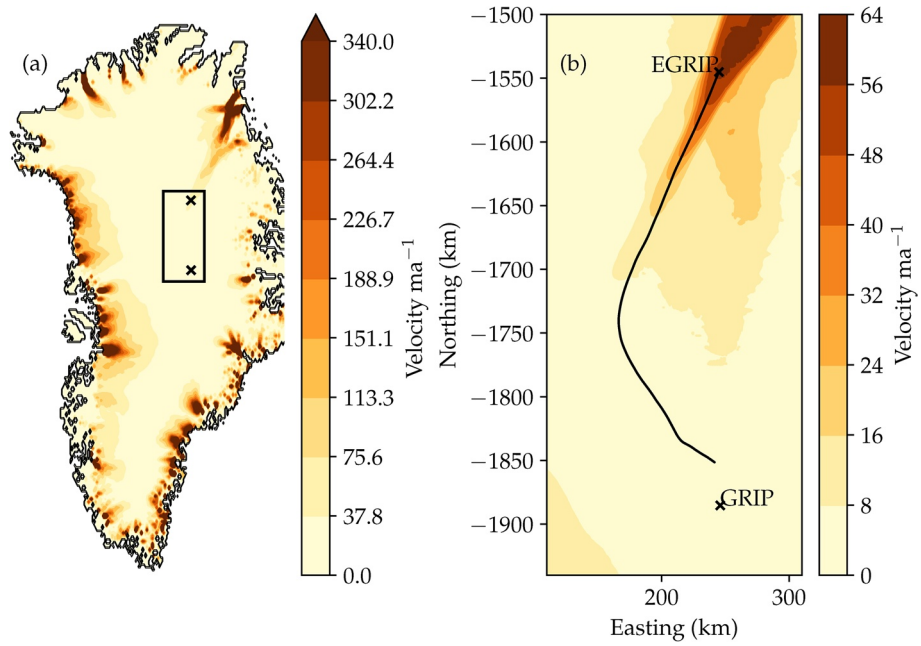

Figure 5. Map of Greenland in (a), showing the velocity magnitude calculated from Joughin et al. (2018) and a magnification in (b), which shows the tracked plan-view path upstream of the East Greenland Ice-core Project (EGRIP) ice-core location. The location of the GRIP core is also shown.

a Dansgaard-Johnson profile (Dansgaard & Johnsen, 1969), being constant for the upper two-thirds of the ice divide, and then decreasing linearly to zero at the ice-bedrock interface. The only input parameters for this method are then the ice thickness at the divide, which for GRIP is 3,029 m; the accumulation rate, which sets the vertical velocity at the surface, is 0.23 a^{-1}, and the data for the temperature profile is given by Johnsen e al. (1995).

3.4. Estimating the Deformation of an Ice Stream

To apply SpecCAF for fabric prediction at EGRIP, we must estimate the three-dimensional path, deformation, and temperature history of the ice along the vertical depth of the drilled ice core. This means that, unlike experiments, and the theoretical exploration of general two-dimensional flow regimes in Richards et al. (2022), the ice parcel undergoes a changing history of deformations as it moves through the ice sheet.

We use velocity data from Joughin et al. (2016, 2018) to determine the velocity field, and velocity gradients at the surface of the ice sheet. First, we use the velocity fields to calculate the horizontally two-dimensional surface particle path (Figure 5) backwards from EGRIP. To estimate the velocity gradients within the ice sheet, we apply the Shallow Stream Approximation (SSA) (MacAyeal, 1989), under which $\partial w/\partial x$, $\partial w/\partial y$ are neglected compared to other strain-rate components on the basis of the thinness of the flow, and the horizontal flow in the upper section of the ice sheet forms an approximate plug flow with negligible vertical shear. In other words, horizontal velocities measured at the surface are applied into the ice sheet to first order.

To determine three-dimensional particle paths that intersect the EGRIP site, we choose different initial locations on the surface particle path, shown as a black curve in Figure 5. Different initial locations along this trajectory will create particle paths that intersect EGRIP at different depths along the ice core. For a given location upstream on this plan-view path, the vertical velocity can be found through the kinematic condition:

$$w_s = -\dot{a} + u_s \frac{\partial h}{\partial s} \tag{8}$$

with $\dot{a}$ the accumulation rate, u_s the surface velocity in the streamline direction and $\partial h/\partial s$ the change in surface height along the streamline, calculated from surface height data (Morlighem et al., 2017). The accumulation rate is chosen such that the final age and depth of an ice parcel at EGRIP match the measured age-depth relationship

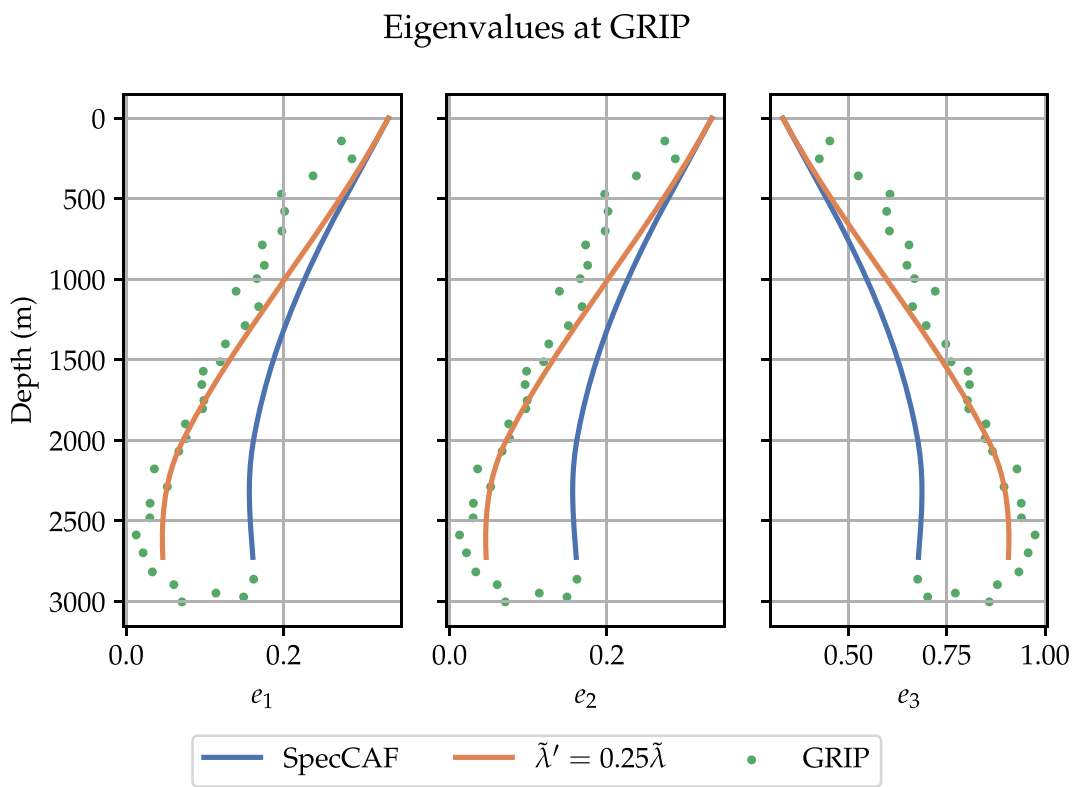

Figure 6. Evolution of fabric tensor eigenvalues at Greenland Ice-core Project (GRIP) with depth for both the experimental parameters (SpecCAF), reduced diffusion to give the correct prediction at here ($\tilde{\lambda}' = 0.25\tilde{\lambda}$) and measurements from GRIP ice cores (data points).

from Gerber et al. (2021). The vertical velocity and, in turn, the three-dimensional particle path can then be found by integration in time. These paths are shown in Figure 7, with the streamline tangent being along the x axis. Pole figures showing model predictions are also shown in this figure, to be discussed in Section 4.2.1.

Data from Prior-Jones et al. (2021) show that the temperature at EGRIP is approximately −30°C to a depth of 1,400 m. As the fabric data used here extend only to a depth of approximately 1,600 m, a temperature of −30°C is used throughout. At this temperature the parameters in the model are $\iota = 1.17$ (controlling lattice rotation), $\tilde{\lambda} = 0.236$ (controlling the effect of rotational recrystallization through diffusion) and $\tilde{\beta} = 1.14$ (controlling the effect of migration recrystallization) (Richards et al., 2021). For these conditions and parameter settings, migration recrystallization is negligible within the model.

As snow accumulates, the ice crystal orientations are initially random, that is, the fabric is isotropic. As the snow compacts into glacial ice, there is a significant component of vertical compression arising from the change in density. This transition is shown by the one larger eigenvalue and two equal-valued smaller eigenvalues at around 110 m in Figure 4, indicative of a vertical single maximum. We include this effect using density profiles with depth from (Vallelonga et al., 2014). This results in a contribution to fabric evolution from the term $\rho^* \nabla \cdot \boldsymbol{u}$ in Equation 2.

4. Results

4.1. Application to an Ice Divide

We first compare model predictions with ice-core data from the GRIP ice divide in Figure 6. The figure compares the eigenvalues of the second-order orientation tensor, which are shown as functions of depth, alongside a range of point measurements from drilled ice cores. As the deformation here is unconfined compression throughout the depth, the fabric forms the expected single-maximum fabric—seen by one larger eigenvalue and two equal-valued smaller ones—orientated vertically.

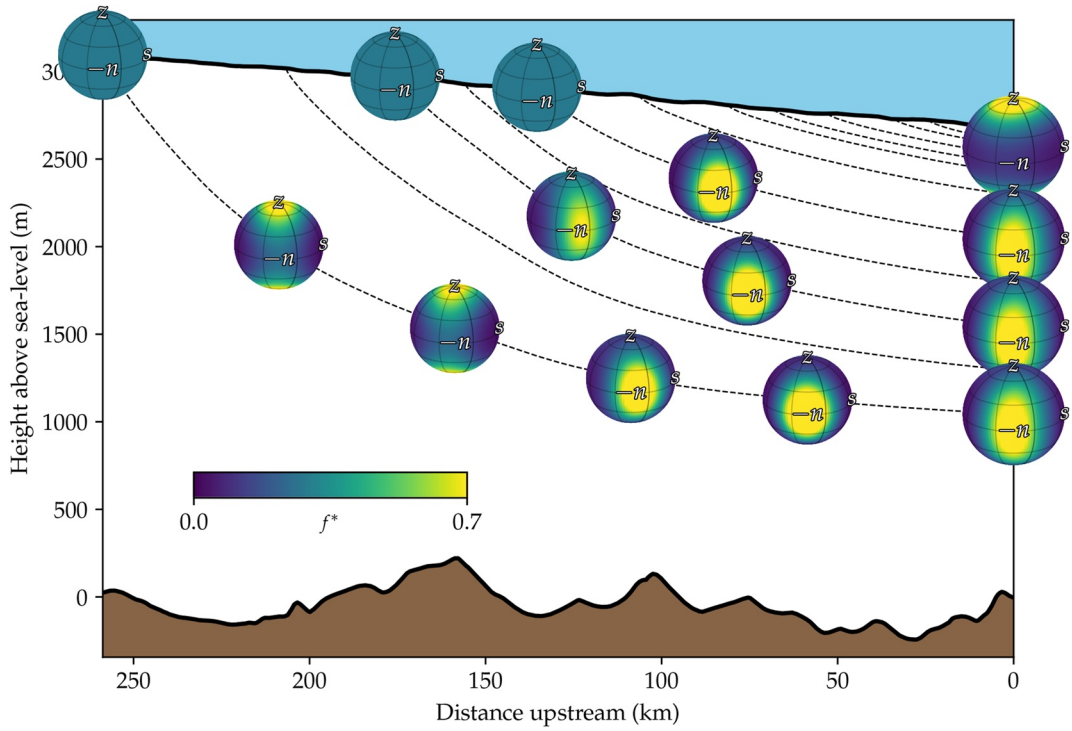

Figure 7. Figure showing streamline paths along the horizontal streamline upstream of East Greenland Ice-core Project (EGRIP). Pole figures are also shown at their corresponding locations, highlighting the fabric development from initially isotropic to what is predicted at the EGRIP drill site. Pole figures are shown with their coordinate system, *s* representing the tangent to the horizontal streamline direction, *z* the vertical, and *n* the normal to the streamline tangent. The brown region represents basal topography.

A perfect single maximum fabric has eigenvalues of 1,0,0. As the single maximum diffuses the eigenvalues tend to 1/3, 1/3, 1/3, which represents an isotropic fabric with no preferred orientation. As can be seen in Figure 6, for the SpecCAF model, using parameters constrained against laboratory experiments, the predictions agree with the general form of the fabric seen at GRIP: a single large eigenvalue indicating a vertical single maximum, which increases in strength with depth. However, SpecCAF predicts a fabric that is more diffuse than observed from the GRIP ice core, because the eigenvalues of the SpecCAF predicted fabric are all closer to 1/3.

Because rotational recrystallization is modeled as a diffusive process, which affects only the fabric strength but not the fabric pattern, in contrast to the process of basal-slip deformation and migration recrystallization, we hypothesize that the effect of rotational recrystallization (controlling diffusion in the model) is strain-rate dependent. As mentioned above, at $T = -30°C$, the model parameters, as constrained by experiments, are $\iota = 1.17$ (controlling lattice rotation), $\tilde{\lambda} = 0.236$ (controlling the effect of rotational recrystallization through diffusion) and $\tilde{\beta} = 1.14$ (controlling the effect of migration recrystallization). For these values, migration recrystallization does not significantly affect the fabric. Thus, we propose that the disparity in fabric strength can be attributed to a dependence of the rate of rotation recrystallization, measured by $\tilde{\lambda}$, on the strain rate. We sought to find the value of $\tilde{\lambda}$ which gives good predictions for this simple case. The reduced value of

$$\tilde{\lambda}' = 0.25\ \tilde{\lambda} \tag{9}$$

was found to give the best fit at the GRIP divide, as can be seen in Figure 6. With this new parameter setting, the model accurately predicts the strength of the vertical single maximum fabric observed there. The result indicates that the effect of rotational recrystallization is reduced by a factor of 0.25 under the characteristic strain rates of ice-sheet flow compared to the strain rates typical in the laboratory.

We note that the strain rates are similar at both GRIP and EGRIP. The mean vertical strain rate at GRIP is $\approx 2 \times 10^{-12}\ s^{-1}$, while mean horizontal strain rates at EGRIP are $\approx 1 \times \sim 10^{-11}\ s^{-1}$, a similar order of magnitude. Therefore, if our hypothesis of strain-rate dependence is correct, the value of $\tilde{\lambda}'$ proposed for natural ice defined by Equation 9 can be anticipated to apply to the context of an ice stream at EGRIP below.

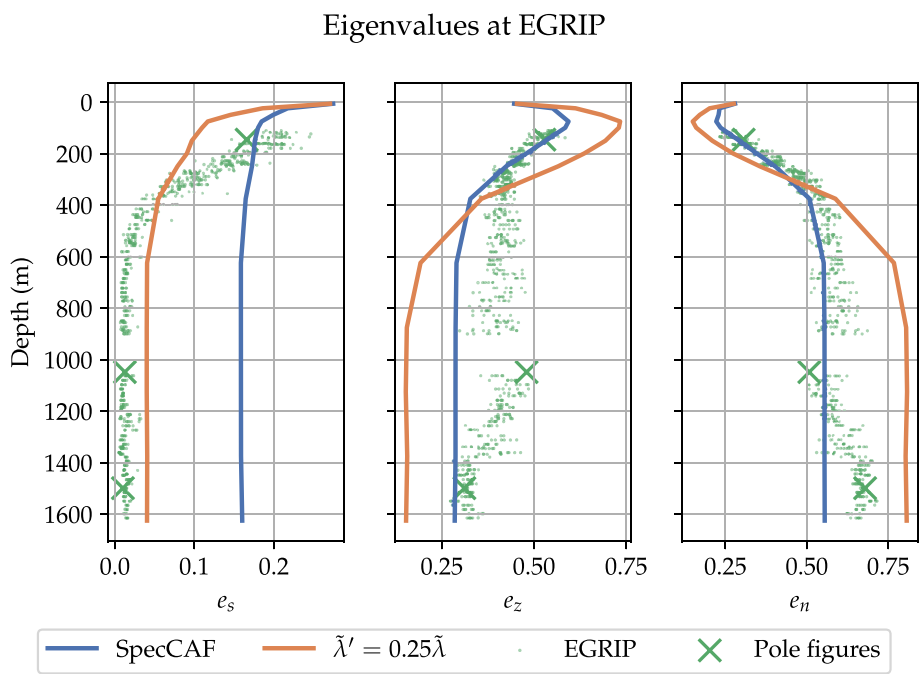

Figure 8. Variation of fabric tensor eigenvalues at East Greenland Ice-core Project (EGRIP) with depth for both the experimental parameters (SpecCAF), reduced diffusion to give the correct prediction at Greenland Ice-core Project (GRIP) ($\tilde{\lambda}' = 0.25\tilde{\lambda}$) and measurements from EGRIP ice cores (data points). The data points corresponding to the pole figures shown in Figures 9 and 10 are highlighted with a cross.

4.2. Application to an Ice Stream

4.2.1. Predicted Fabric Development and Evolution

Results are presented comparing the predictions of the model with the eigenvalues obtained from ice cores at EGRIP, for both the original experimentally calibrated parameters, and the set that includes the adjusted value of $\tilde{\lambda}'$ given by Equation 9. As the deformation is changing upstream of EGRIP, the fabric pattern changes and there are three characteristics we can compare between observations and model predictions: (a) the fabric pattern (cf. Figure 3); (b) the orientation of the fabric pattern (constrained recently in observations for the first time (Westhoff et al., 2021); and (c) the fabric strength measured by the eigenvalues of the second-order orientation tensor.

The predicted paths upstream of EGRIP and the fabric evolution along those paths are shown in Figure 7 for the original parameters, where the x axis is the distance s along the horizontal streamline path shown in Figure 5. This allows the change in fabric pattern through different deformation regimes to be visualized. At the surface, the fabric at the beginning of each path is initially isotropic. Far upstream, the model initially predicts the development of a vertical single-maximum fabric, attributable to dominant vertical compression in this region where there is comparatively less acceleration causing horizontal velocity gradients. For all but the highest streamlines, the model predicts that either horizontal maximum or girdle fabrics develop subsequently under the combined effects of acceleration in the flow direction and cross-flow shear. The highest (shortest) streamline shown predicts a vertical single maximum fabric at EGRIP; this can be attributed to the dominant vertical compression in this region due to densification of the firn layer.

4.2.2. Comparison With Ice-Core Data From an Ice Stream

Using our approximations for the flow fields, we compare our model predictions to observations from the EGRIP ice core (Stoll et al., 2021) (Figure 8). As in Figure 6, the figure compares the eigenvalues of the second-order orientation tensor with depth against ice-core measurements. We show predictions for both the original, laboratory-calibrated parameters, and the adjusted set that includes the reduced value of the recrystallization coefficient $\left(\tilde{\lambda}' = 0.25\ \tilde{\lambda}\right)$ proposed in Equation 9. We also show pole figures showing fabrics in the firn-influenced layer (Figure 9), and at two deeper depths (1,048 m and 1,499 m in Figure 10). These are chosen to illustrate the range of fabrics observed at EGRIP, and are highlighted in Figure 8 by crosses. The observed fabrics from EGRIP

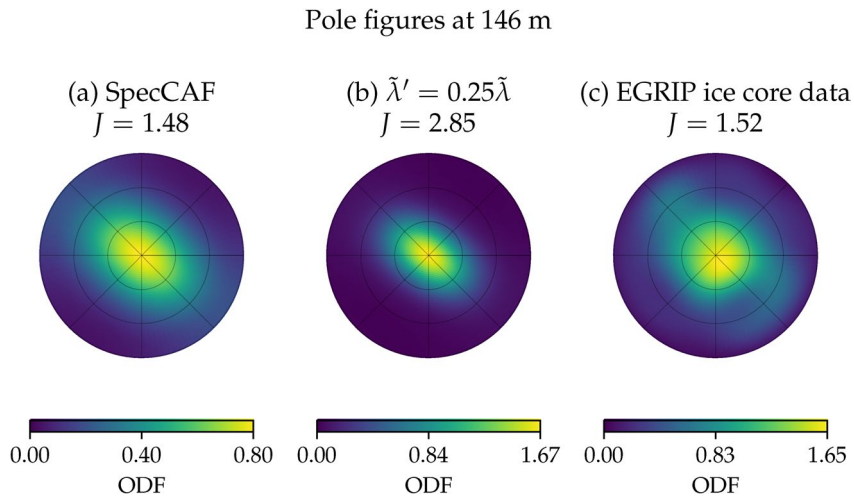

Figure 9. Pole figures at the shallow depth of 146 m, for (a) the original model, (b) the model with the effect of rotational recrystallization reduced, and (c) from *c* axis orientations measured from a single ice-core sample. At this shallow depth, the vertical single maximum is produced due to densification in the firn layer. The *J* index (Equation 10) is also shown.

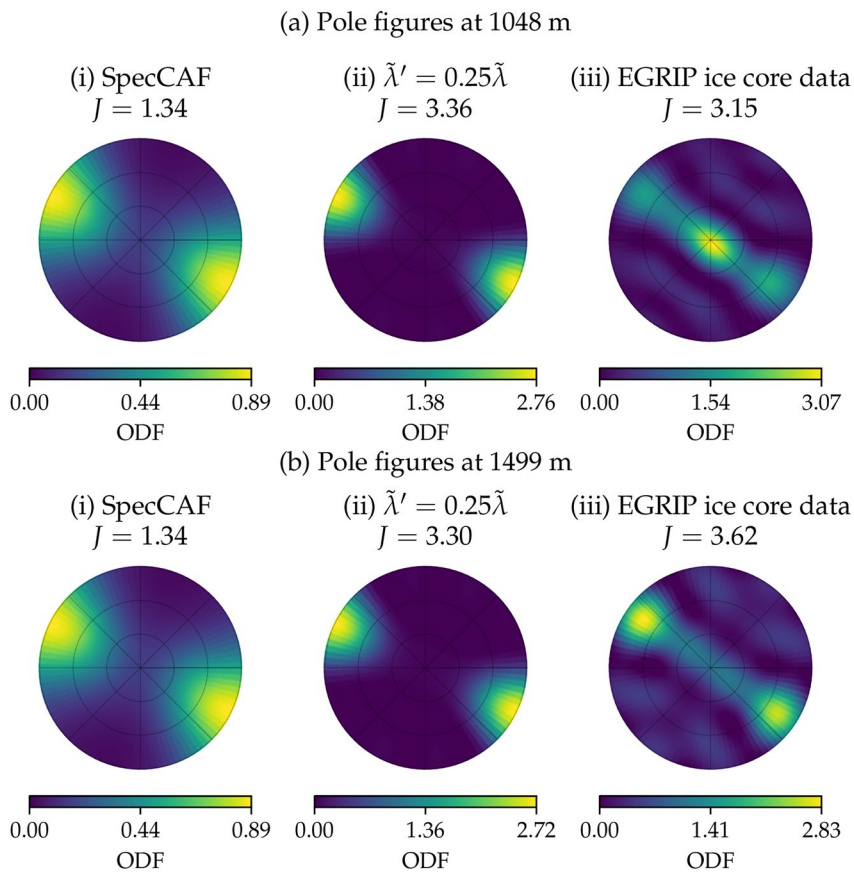

Figure 10. Pole figures at a depth of (a) 1,048 m and (b) 1,449 m, for (i) the original model, (ii) the model with the effect of rotational recrystallization reduced, and (iii) from *c* axis orientations measured from a single ice-core sample. The East Greenland Ice-core Project (EGRIP) pole figures have been rotated to match the girdle angle of 125° found by Westhoff et al. (2021). The *J* index (Equation 10) is also shown.

in Figure 10 are also rotated to the average orientation over the depth found by Westhoff et al. (2021), allowing the fabric orientation to be compared as well. The J index is also calculated from the pole figure data, defined by:

$$J = \int_{S^2} \left(\frac{\rho^*}{\rho} \right)^2 \mathrm{d}\boldsymbol{n} \tag{10}$$

This is a measure of fabric strength ranging from 1 for isotropic fabrics to ∞ for perfect single maximum fabrics (Bunge, 1969).

We first examine the fabrics in the upper 300 m at EGRIP, where a vertical single-maximum is predicted by both sets of model parameters, and is also observed in the ice core. As noted above, this fabric can be attributed to compaction in the firn layer ($\nabla \cdot \boldsymbol{u} \neq 0$), where the snow is compressed into ice. Pole figures showing both the experimental parameters (SpecCAF), the reduced set $\left(\tilde{\lambda}' = 0.25\ \tilde{\lambda}\right)$ and an orientation distribution function produced from the measured c-axis orientations in the ice core are shown in Figure 9. The experimental parameters (Figure 9a) accurately predict the vertical single maximum observed (Figure 9c), showing densification can explain these fabrics to leading order. However, processes occurring in the firn layer are likely to be quite different from the rest of the ice sheet.

Below the firn layer, fabric evolution is dominated by incompressible deformations inside the ice sheet. The modeled eigenvalues in Figure 8 show that below a depth of approximately 500 m, the fabric becomes mostly invariant with depth. Both sets of parameters and ice-core data show two larger eigenvalues and one smaller one, particularly for the ice-core observations and the reduced parameter set, where the smallest eigenvalue is close to zero (Figure 8). This pattern of eigenvalues is indicative of a girdle fabric, which can be seen in the pole figures from the predicted and observed fabrics (Figure 10).

Figure 10 shows that there is good agreement between observations and both sets of parameters for the orientation of the fabric, which is perpendicular to the flow direction. The fabric pattern at 1,048 m (Figure 10aiii) is close to a perfect girdle, whereas the observed fabric pattern at 1,499 m (Figure 10biii) is closer to a horizontal maximum. This variation is likely due to changes in deformation with depth not included in our leading-order flow model. The experimentally calibrated parameters predict a fabric pattern that is closer to a horizontal maximum. The parameter settings with the reduced recrystallization coefficient $\left(\tilde{\lambda}' = 0.25\ \tilde{\lambda}\right)$ forms a more defined horizontal maximum. Consequently, the model achieves a partial agreement with EGRIP when comparing the fabric pattern.

The fabric strength can be measured more precisely by the J index, calculated for the pole figures in Figure 10, than the eigenvalues. While the experimental parameters result in an underprediction of the fabric strength, the fabric strength of the second set of parameters agrees with observations at EGRIP.

In summary, of our three metrics (orientation, pattern, and fabric strength), the model agrees well for the fabric orientation, and partially for the fabric pattern. This shows that our current understanding of fabric evolution through dislocation creep, encapsulated by the model, can work in ice streams. The model under-estimates the strength of the fabric, but this can be rectified by reducing the effect of rotational recrystallization in the model. Our results have therefore revealed both a key quantitative difference between fabrics produced in the laboratory and in ice sheets, whilst demonstrating that the continuum theory can be modified to yield better agreement with observations following a simple reduction in the rotational recrystallization parameter $\tilde{\lambda}$.

5. Discussion

5.1. Characteristic Fabrics of Ice Streams

The results provide some of the first direct comparison between fabrics from an active ice stream and model predictions. Further, our results provide new direct quantitative comparisons between observations and an experimentally calibrated model surrogate, thereby allowing the gap between fabrics produced under experimental and observational strain rates to be bridged.

Outside of the upper depths influenced by the compaction of the firn layer, the fabric pattern observed at EGRIP and predicted by the different model parameters is, to leading order, invariant with depth and lies between a horizontal maximum and a girdle, which is always orientated perpendicular to the flow direction. These fabric

patterns can be explained by different deformation regimes. The girdle pattern will be produced by dislocation glide along the basal plane under a deformation of unconfined extension, with the plane of the girdle perpendicular to the direction of extension. In contrast, a horizontal-maximum pattern is likely caused by a component of simple shear across the streamline. These patterns have been fitted to seismic data taken from ice streams and shelves (Kufner et al., 2023; Lutz et al., 2020; Smith et al., 2017), although Kufner et al. (2023) finds other possible fabrics also fit their data. Thus, we consider this girdle/horizontal-maximum pattern orientated perpendicular to the local flow direction to be the characteristic fabric of ice streams, just as a vertical single maximum or tight girdle fabric is characteristic of ice divides (Faria et al., 2014).

5.2. Utilizing Modeling for Comparing Experiments and Ice Sheets

Richards et al. (2021) showed that the model employed here accurately predicts fabrics at experimental strain rates (approximately 10^{-5} s^{-1}). The strain rate at EGRIP is of order 10^{-11} s^{-1}, and the strain rate at GRIP is of order 10^{-12} s^{-1}. It is an open question how fabrics vary across this range of strain rates, not only for ice but for materials such as olivine where natural strain rates are likewise much lower than can be reached in experiments. Our findings reveal that the fabric predicted with the experimental parameters is significantly weaker than observed in the geophysical setting. For example, the *J* index predicted by the experimental parameters at EGRIP is around 1.35, whereas observations show a *J* index of around 3.4 (Figure 10). Therefore, we can conclude that fabrics are stronger at the lower strain rates seen in ice sheets compared to the faster strain rates in the laboratory, for the same applied strain. This trend can also be seen over the range of experimental strain rates (Figure 3 in Richards et al. (2021)).

Our analysis highlights both the benefits and drawbacks of laboratory experiments. Although the fabrics generated in experimental environments generally exhibit similar patterns and orientations to those found in nature, as demonstrated by the qualitative agreements shown here, our results demonstrate a disparity in fabric strength between the two settings. Conducting laboratory experiments at strain rates comparable to ice streams is not feasible, as it would necessitate decades to complete a single experiment. The disparity between experimental and geodynamic strain rates is yet more extreme for olivine, where experiments also take place at around 10^{-5} s^{-1} (e.g., Hansen et al., 2016), but the mantle deforms around 10^{-16} s^{-1}. As such, modeling serves as a crucial tool to bridge this gap.

Better agreement between the predictions and observed fabric strength for both the ice stream and divide is found by reducing the coefficient controlling rotational recrystallization (modeled as a diffusion in orientation space) by a factor of ≈4. This suggests that the process of rotational recrystallization is strain-rate dependent. Other processes that act to strengthen the fabric may also be relatively more active at lower strain rates. This includes grain boundary migration driven by surface energy, rather than dislocation density, which will result in grain growth. Post deformation grain growth has been shown to produce stronger fabrics (e.g., Piazolo et al., 2010).

5.3. Implications for Microstructure Deformation Mechanisms in Ice Stream Flow

While experiments provide rich data sets to determine the microstructural processes occurring, such as dislocation creep or grain boundary sliding, it is more difficult to observe this in nature. In ice, it remains an open question whether ice-sheet flow can be entirely explained by dislocation creep (incorporating basal-slip deformation, rotational recrystallization, and migration recrystallization), as represented by the fabric model utilized in this study, or whether other processes, such as grain boundary sliding, play a significant role. Goldsby and Kohlstedt (2001) posited that grain boundary sliding is the primary deformation process in ice sheets. Although this is unlikely to be entirely accurate (Duval & Montagnat, 2002), recent evidence has emerged supporting the occurrence of grain boundary sliding in laboratory experiments (e.g., Craw et al., 2018). Deformation by grain boundary sliding alone does not produce a fabric (Duval & Montagnat, 2002; Zhang et al., 1994), and an increased contribution of grain boundary sliding to deformation would result in a weaker fabric. The modeling in this paper reveals that the ice stream fabrics are stronger than expected from laboratory experiments. Given that grain boundary sliding weakens the fabric, the results indicate that deformation in ice streams and ice sheets as a whole is predominantly governed by dislocation creep. Grain boundary sliding may be active at laboratory strain rates where the observed fabric is weaker than ice sheets. This is contrary to the proposal of Goldsby and Kohlstedt (2001) that grain boundary sliding dominates at low strain rates and dislocation creep at higher rates.

5.4. Timescales for Fabrics to Adjust to New Deformations

The duration for which fabrics retain their "history," that is, the speed at which fabrics adapt to changes in deformation and the extent to which upstream deformation must be considered, is currently an open question, with estimates only available on the local scale (e.g., McCormack et al., 2022). While providing a robust measure of this duration is beyond the scope of this paper, the tracking of ice parcels in this work allows insights for the case of EGRIP. The observed fabric at EGRIP, as well as the model predictions using the experimental parameters, do not vary significantly for depths below approximately 500 m. The streamline that ends at this depth starts 150 km upstream and takes a total time of around 4,000 years to travel from the surface to EGRIP (as calculated through streamline integration). We have assumed the vertical variation in the deformation is negligible over the depth examined.

Therefore, the depth of a parcel of ice at EGRIP is a proxy for the total time that it has experienced deformation. As fabrics below a depth of 500 m at EGRIP, corresponding to a time of 4,000 years, show no change in final fabric, we can say that any deformation history older than 4,000 years is irrelevant for the case of EGRIP under our modeling assumptions. Lilien et al. (2021) found that changes in deformation might impact fabric for approximately 1,000 to 10,000 years, which broadly aligns with our results. These timescales will change with the rate of deformation undergone with the fabric, such that this result can only be applied to EGRIP. Furthermore, we have assumed that the ice stream remains constant over time. Franke et al. (2022) however suggest the NEGIS (the ice stream EGRIP is within) has shifted during the Holocene (within the last 11,700 years).

5.5. Predicting Fabrics in Nature: Future Work in Ice and Other Polycrystalline Materials

Since the model used here, SpecCAF, does not explicitly include the microstructure and only tracks changes in the fabric distribution function within an empirically calibrated model, we can only interpret, rather than know precisely, what microstructural deformation and recrystallization processes are taking place. Models that directly solve for the ice microstructure do exist (e.g., Llorens et al., 2022). Although these models are more computationally demanding and cannot accommodate changing deformations as easily as models like the one used here or in Lilien et al. (2021), they can provide another benchmark, alongside observations, for the model utilized in this study by simulating grain interactions directly.

In this work, we estimated the upstream ice deformation with a simple flow line model of ice dynamics combined with satellite data, in contrast to other work which couples fabric evolution to an ice-sheet simulation (Gerber et al., 2023). In particular, we have a vertically invariant deformation over the depth examined (although the deformation experienced by an ice parcel moving through the ice stream does of course change). We have also assumed that the temperature is approximately invariant over the depth examined, consistent with observations. Although the observed fabric at EGRIP is mostly invariant with depth (Figure 8), these assumptions mean this work cannot represent the detailed features seen at depth in ice-core observations, such as the slight increase in the largest eigenvalue e_n at 1,200 m. These features, which have only a small effect on the observed fabric, may be caused by features not included in this study such as folding in the ice. This remains an open question for future study.

In this work we have assumed that any change in the effect of recrystallization on the fabric with depth is driven by changes in the temperature and strain-rate/stress experienced by the ice parcel at that depth. Other physics, such as the effects of grain size or impurities present in the ice sheet may also affect the activity of different recrystallization processes, and significant depth dependence has been observed from ice cores (Alley et al., 1986; Azuma et al., 2000; Lipenkov et al., 1989; Thomas et al., 2021). Examining these processes is beyond the scope of the current model.

We attempted to find a set of parameters that gave the correct girdle fabric pattern and fabric strength observed at EGRIP. However, we found that there was not a set of parameters that provided a good fit over the entire depth. This highlights that modification of the model equations may be needed. One possible area for improvement is in modeling the effect of basal-slip deformation. Placidi et al. (2010) and Richards et al. (2021) assume a linear relationship between this effect and the deformation tensor $\mathbf{D}_{ij}$, whereas in ice the stress may play a significant role in determining the basal-slip deformation (Lebensohn et al., 2004).

Ice makes an excellent model material for studying the evolution of fabrics in general (Wilson et al., 2014). The approach of tracking particle paths to coincide with observations provides a method to constrain fabric evolution

models in natural conditions. This presents a pathway for including fabric evolution models into large-scale flow models in geodynamics (e.g., Bangerth et al., 2022; Mansour et al., 2020). Further work is required to extend the mathematical equations to multiple slip systems necessary for modeling the fabrics of many polycrystalline materials.

6. Conclusions

In this study, we have presented the first attempt to predict ice fabrics directly from real-world ice stream velocity data in order to compare to ice-core observations. By using the SpecCAF model, which is constrained against laboratory experiments, we have both tested the predictions of the model as well as used the model as a surrogate to compare between laboratory experiments and natural fabrics, formed at much lower strain rates, thereby bridging the gap in interpreting experimental and observational fabrics.

The method of combining satellite data with fabric modeling allows us to accurately predict the fabric pattern and orientation in the ice stream. As this method does not require coupling to flow simulations, it can be readily applied to other ice-sheet locations.

Our results indicate that fabrics are stronger at natural strain rates, which are several orders of magnitude smaller than those seen in the laboratory. This has implications not only for ice, but for olivine in the mantle, where models are also constrained against experiments. By using modeling as a surrogate, we compare the change in different processes like rotational recrystallization across the strain-rate range, bridging this gap. We find that reducing the effect of rotational recrystallization to a quarter of the laboratory-calibrated value agrees with ice divide observations. Furthermore, the fact that fabrics are stronger at lower strain rates suggests that dislocation creep dominates deformation in natural ice conditions.

For EGRIP, our model predicts the development of a horizontal-maximum fabric, oriented perpendicular to the flow, when run with an adjusted recrystallization parameter. This fabric is seen in other ice streams such as Rutford (Smith et al., 2017). However, this predicted pattern does not precisely agree with the girdle/horizontal maximum observed at EGRIP. Further work needs to be done to capture the precise details of this fabric, but our current modeling captures its leading-order form.

The modeling also allows new insights into the formation of fabrics in strain localized zones like EGRIP. Approximately 6,000 years of deformation history is required to yield accurate predictions, with changes in deformation older than this having little effect. A quantitative (modeling) approach, rather than a qualitative interpretation of local deformation and fabric patterns, is necessary in order to interpret ice fabrics undergoing changing deformations reliably. The methodology presented in this paper provides a new means to test and constrain fabric evolution models in dynamic, natural conditions.

Acknowledgments
This research was supported by the Australian Research Council Special Research Initiative, Australian Centre for Excellence in Antarctic Science (Project Number SR200100008), as well as UK Engineering and Physical Sciences Research Council (EPSRC) Grant EP/L01615X/1 for the University of Leeds centre for doctoral training in fluid dynamics. Nicolas Stoll gratefully acknowledges funding from the Helmholtz Young Investigator Group "The effect of deformation mechanisms on ice-sheet dynamics" (VH-NG-802). EastGRIP is directed and organized by the Centre for Ice and Climate at the Niels Bohr Institute, University of Copenhagen. It is supported by funding agencies and institutions in Denmark (A. P. Møller Foundation, University of Copenhagen), the USA (US National Science Foundation, Office of Polar Programs), Germany (Alfred Wegener Institute, Helmholtz Centre for Polar and Marine Research), Japan (National Institute of Polar Research and Arctic Challenge for Sustainability), Norway (University of Bergen, Trond Mohn Foundation), Switzerland (Swiss National Science Foundation), France (French Polar Institute Paul-Émile Victor, Institute for Geosciences and Environmental Research), Canada (University of Manitoba), and China (Chinese Academy of Sciences, Beijing Normal University).

Data Availability Statement

The EGRIP eigenvalue data are available on PANGAEA, https://doi.org/10.1594/PANGAEA.949248 (Weikusat et al., 2022). EGRIP density data with depth was digitized from Vallelonga et al. (2014). The GRIP eigenvalue data were digitized from Thorsteinsson et al. (1997). GRIP temperature data with depth is available at https://doi.org/10.1594/PANGAEA.89007 (Johnsen, 2003). Code which can reproduce the figures in this paper is available at https://doi.org/10.5281/zenodo.10020144 (Richards, 2023), which contains code to extract the relevant data from velocity maps of Greenland at https://doi.org/10.5067/QUA5Q9SVMSJG (Joughin et al., 2016) and from surface height data, https://doi.org/10.5067/FPSU0V1MWUB6 (Morlighem, 2022). The EGRIP age-depth relationship is taken from the supplement of Gerber et al. (2021). The pole figure data from EGRIP are available at https://doi.org/10.5281/zenodo.8015759 (Stoll & Weikusat, 2023). The Specfab fabric solver is available at https://github.com/nicholasmr/specfab.

References

Alley, R. B., Perepezko, J., & Bentley, C. (1986). Grain growth in polar ice: I. Theory. *Journal of Glaciology*, *32*(112), 415–424. https://doi.org/10.3189/S0022143000012120

Azuma, N., Wang, Y., Yoshida, Y., Narita, H., Hondoh, T., Shoji, H., & Watanabe, O. (2000). Crystallographic analysis of the Dome Fuji ice core. In T. Hondoh (Ed.), *Physics of ice core reconis*. Hokkaido University Press.

Bangerth, W., Dannberg, J., Fraters, M., Gassmoeller, R., Glerum, A., Heister, T., et al. (2022). ASPECT v2.4.0. *Zenodo*. https://doi.org/10.5281/zenodo.6903424

Behrmann, J., & Mainprice, D. (1987). Deformation mechanisms in a high-temperature quartz-feldspar mylonite: Evidence for superplastic flow in the lower continental crust. *Tectonophysics*, *140*(2), 297–305. https://doi.org/10.1016/0040-1951(87)90236-8

Bennett, M. (2003). Ice streams as the arteries of an ice sheet: Their mechanics, stability and significance. *Earth-Science Reviews*, *61*(3–4), 309–339. https://doi.org/10.1016/S0012-8252(02)00130-7

Bunge, H. J. (1969). *Texture analysis in materials science: Mathematical models*. Butterworths. https://doi.org/10.1016/C2013-0-11769-2

Castelnau, O., Duval, P., Lebensohn, R. A., & Canova, G. R. (1996). Viscoplastic modeling of texture development in polycrystalline ice with a self-consistent approach: Comparison with bound estimates. *Journal of Geophysical Research*, *101*(B6), 13851–13868. https://doi.org/10.1029/96JB00412

Castelnau, O., Thorsteinsson, T., Kipfstuhl, J., Duval, P., & Canova, G. R. (1996). Modelling fabric development along the GRIP ice core, central Greenland. *Annals of Glaciology*, *23*, 194–201. https://doi.org/10.3189/S0260305500013446

Coble, R. L. (1963). A model for boundary diffusion controlled creep in polycrystalline materials. *Journal of Applied Physics*, *34*(6), 1679–1682. https://doi.org/10.1063/1.1702656

Craw, L., Qi, C., Prior, D. J., Goldsby, D. L., & Kim, D. (2018). Mechanics and microstructure of deformed natural anisotropic ice. *Journal of Structural Geology*, *115*, 152–166. https://doi.org/10.1016/j.jsg.2018.07.014

Dansgaard, W., & Johnsen, S. J. (1969). A flow model and a time scale for the ice core from Camp Century, Greenland. *Journal of Glaciology*, *8*(53), 215–223. https://doi.org/10.3189/S0022143000031208

Dansgaard, W., Johnsen, S. J., Møller, J., & Langway, C., Jr. (1969). One thousand centuries of climatic record from Camp Century on the Greenland ice sheet. *Science*, *166*(3903), 377–381. https://doi.org/10.1126/science.166.3903.377

Drury, M., Humphreys, F., & White, S. (1985). Large strain deformation studies using polycrystalline magnesium as a rock analogue. Part II: Dynamic recrystallisation mechanisms at high temperatures. *Special Issue Experiments in Solid State Physics Relevant to Lithospheric Dynamics*, *40*(3), 208–222. https://doi.org/10.1016/0031-9201(85)90131-1

Duval, P., Ashby, M. F., & Anderman, I. (1983). Rate-controlling processes in the creep of polycrystalline ice. *The Journal of Physical Chemistry*, *87*(21), 4066–4074. https://doi.org/10.1021/j100244a014

Duval, P., & Montagnat, M. (2002). Comment on "Superplastic deformation of ice: Experimental observations" by D. L. Goldsby and D. L. Kohlstedt. *Journal of Geophysical Research*, *107*(B4), 2082. https://doi.org/10.1029/2001JB000946

Faria, S. H. (2006a). Creep and recrystallization of large polycrystalline masses. I. General continuum theory. *Proceedings of the Royal Society A: Mathematical, Physical and Engineering Science*, *462*(2069), 1493–1514. https://doi.org/10.1098/rspa.2005.1610

Faria, S. H. (2006b). Creep and recrystallization of large polycrystalline masses. III. Continuum theory of ice sheets. *Proceedings of the Royal Society A: Mathematical, Physical and Engineering Sciences*, *462*(2073), 2797–2816. https://doi.org/10.1098/rspa.2006.1698

Faria, S. H., Weikusat, I., & Azuma, N. (2014). The microstructure of polar ice. Part II: State of the art. *Microdynamics of Ice*, *61*, 21–49. https://doi.org/10.1016/j.jsg.2013.11.003

Franke, S., Bons, P. D., Westhoff, J., Weikusat, I., Binder, T., Streng, K., et al. (2022). Holocene ice-stream shutdown and drainage basin reconfiguration in northeast Greenland. *Nature Geoscience*, *15*(12), 995–1001. https://doi.org/10.1038/s41561-022-01082-2

Gagliardini, O., Zwinger, T., Gillet-Chaulet, F., Durand, G., Favier, L., de Fleurian, B., et al. (2013). Capabilities and performance of Elmer/Ice, a new-generation ice sheet model. *Geoscientific Model Development*, *6*(4), 1299–1318. https://doi.org/10.5194/gmd-6-1299-2013

Gerber, T. A., Hvidberg, C. S., Rasmussen, S. O., Franke, S., Sinnl, G., Grinsted, A., & Jansen, D. (2021). Upstream flow effects revealed in the EastGRIP ice core using Monte Carlo inversion of a two-dimensional ice-flow model. *The Cryosphere*, *15*(8), 3655–3679. https://doi.org/10.5194/tc-15-3655-2021

Gerber, T. A., Lilien, D. A., Rathmann, N. M., Franke, S., Young, T. J., Valero-Delgado, F., et al. (2023). Crystal orientation fabric anisotropy causes directional hardening of the Northeast Greenland Ice Stream. *Nature Communications*, *14*(1), 2653. https://doi.org/10.1038/s41467-023-38139-8

Glen, J. W. (1968). The effect of hydrogen disorder on dislocation movement and plastic deformation of ice. *Physik der kondensierten Materie*, *7*(1), 43–51. https://doi.org/10.1007/BF02422799

Gödert, G. (2003). A mesoscopic approach for modelling texture evolution of polar ice including recrystallization phenomena. *Annals of Glaciology*, *37*, 23–28. https://doi.org/10.3189/172756403781815375

Goldsby, D. L., & Kohlstedt, D. L. (2001). Superplastic deformation of ice: Experimental observations. *Journal of Geophysical Research*, *106*(B6), 11017–11030. https://doi.org/10.1029/2000JB900336

Gow, A. J. (1961). Deep core studies of the accumulation and densification of snow at Byrd Station and Little America V, Antarctica. (CRREL Res. Rep.). Cold Regions Research and Engineering Laboratory. Retrieved from https://hdl.handle.net/11681/5803

Graham, F. S., Morlighem, M., Warner, R. C., & Treverrow, A. (2018). Implementing an empirical scalar constitutive relation for ice with flow-induced polycrystalline anisotropy in large-scale ice sheet models. *The Cryosphere*, *12*(3), 1047–1067. https://doi.org/10.5194/tc-12-1047-2018

Hansen, L. N., Warren, J. M., Zimmerman, M. E., & Kohlstedt, D. L. (2016). Viscous anisotropy of textured olivine aggregates. Part 1: Measurement of the magnitude and evolution of anisotropy. *Earth and Planetary Science Letters*, *445*, 92–103. https://doi.org/10.1016/j.epsl.2016.04.008

Herring, C. (1950). Diffusional viscosity of a polycrystalline solid. *Journal of Applied Physics*, *21*(5), 437–445. https://doi.org/10.1063/1.1699681

Humphreys, F., & Hatherly, M. (2004). *Recrystallization and related Annealig Phenomena* (2nd ed.). Pergamon.

Jiang, Z., Prior, D. J., & Wheeler, J. (2000). Albite crystallographic preferred orientation and grain misorientation distribution in a low-grade mylonite: Implications for granular flow. *Journal of Structural Geology*, *22*(11), 1663–1674. https://doi.org/10.1016/S0191-8141(00)00079-1

Johnsen, S. J. (2003). GRIP temperature profile. *PANGAEA*. https://doi.org/10.1594/PANGAEA.89007

Johnsen, S. J., Dahl-Jensen, D., Dansgaard, W., & Gundestrup, N. (1995). Greenland palaeotemperatures derived from GRIP bore hole temperature and ice core isotope profiles. *Tellus B: Chemical and Physical Meteorology*, *47*(5), 624–629. https://doi.org/10.3402/tellusb.v47i5.16077

Joughin, I., Smith, B., & Howat, I. (2016). *MEaSUREs Multi-year Greenland ice sheet velocity Mosaic, Version 1*. NASA National Snow and Ice Data Center Distributed Active Archive Center. https://doi.org/10.5067/QUA5Q9SVMSJG

Joughin, I., Smith, B. E., & Howat, I. M. (2018). A complete map of Greenland ice velocity derived from satellite data collected over 20 years. *Journal of Glaciology*, *64*(243), 1–11. https://doi.org/10.1017/jog.2017.73

Kufner, S.-K., Wookey, J., Brisbourne, A. M., Martín, C., Hudson, T. S., Kendall, J. M., & Smith, A. M. (2023). Strongly depth-dependent ice fabric in a fast-flowing Antarctic ice stream revealed with Icequake observations. *Journal of Geophysical Research: Earth Surface*, *128*, e2022JF006853. https://doi.org/10.1029/2022JF006853

Lebensohn, R. A., Liu, Y., & Castañeda, P. P. (2004). Macroscopic properties and field fluctuations in model power-law polycrystals: Full-field solutions versus self-consistent estimates. *Proceedings of the Royal Society of London. Series A: Mathematical, Physical and Engineering Sciences*, *460*(2045), 1381–1405. https://doi.org/10.1098/rspa.2003.1212

Lilien, D. A., Rathmann, N. M., Hvidberg, C. S., & Dahl-Jensen, D. (2021). Modeling ice-crystal fabric as a proxy for ice-stream stability. *Journal of Geophysical Research: Earth Surface*, *126*, e2021JF006306. https://doi.org/10.1029/2021JF006306

Lipenkov, V., Barkov, N., Duval, P., & Pimienta, P. (1989). Crystalline texture of the 2083 m ice core at Vostok Station, Antarctica. *Journal of Glaciology*, *35*(121), 392–398. https://doi.org/10.3189/S0022143000009321

Llorens, M.-G., Griera, A., Bons, P. D., Weikusat, I., Prior, D. J., Gomez-Rivas, E., et al. (2022). Can changes in deformation regimes be inferred from crystallographic preferred orientations in polar ice? *The Cryosphere*, *16*(5), 2009–2024. https://doi.org/10.5194/tc-16-2009-2022

Lutz, F., Eccles, J., Prior, D. J., Craw, L., Fan, S., Hulbe, C., et al. (2020). Constraining ice Shelf anisotropy using shear wave splitting measurements from active-source borehole seismics. *Journal of Geophysical Research: Earth Surface*, *125*, e2020JF005707. https://doi.org/10.1029/2020JF005707

MacAyeal, D. R. (1989). Large-scale ice flow over a viscous basal sediment: Theory and application to ice stream B, Antarctica. *Journal of Geophysical Research*, *94*(B4), 4071–4087. https://doi.org/10.1029/JB094iB04p04071

Mansour, J., Giordani, J., Moresi, L., Beucher, R., Kaluza, O., Velic, M., et al. (2020). Underworld2: Python geodynamics modelling for desktop, HPC and cloud. *Journal of Open Source Software*, *5*(47), 1797. https://doi.org/10.21105/joss.01797

McCormack, F. S., Warner, R. C., Seroussi, H., Dow, C. F., Roberts, J. L., & Treverrow, A. (2022). Modeling the deformation regime of Thwaites glacier, west Antarctica, using a simple flow relation for ice anisotropy (ESTAR). *Journal of Geophysical Research: Earth Surface*, *127*, e2021JF006332. https://doi.org/10.1029/2021JF006332

National Snow and Ice Data Center Distributed Active Archive Center. https://doi.org/10.5067/FPSU0V1MWUB6

Montagnat, M., Buiron, D., Arnaud, L., Broquet, A., Schlitz, P., Jacob, R., & Kipfstuhl, S. (2012). Measurements and numerical simulation of fabric evolution along the Talos Dome ice core, Antarctica. *Earth and Planetary Science Letters*, *357–358*, 168–178. https://doi.org/10.1016/j.epsl.2012.09.025

Morlighem, M., Williams, C. N., Rignot, E., An, L., Arndt, J. E., Bamber, J. L., et al. (2017). BedMachine v3: Complete bed topography and ocean bathymetry mapping of Greenland from multibeam echo sounding combined with mass conservation. *Geophysical Research Letters*, *44*, 11051–11061. https://doi.org/10.1002/2017GL074954

Paterson, W. S. B. (1999). *The physics of glaciers* (3rd ed.). Pergamon.

Piazolo, S., Jessell, M. W., Bons, P. D., Evans, L., & Becker, J. K. (2010). Numerical simulations of microstructures using the Elle platform: A modern research and teaching tool. *Journal of the Geological Society of India*, *75*(1), 110–127. https://doi.org/10.1007/s12594-010-0028-6

Piazolo, S., Montagnat, M., & Blackford, J. R. (2008). Sub-structure characterization of experimentally and naturally deformed ice using cryo-EBSD. *Journal of Microscopy*, *230*(3), 509–519. https://doi.org/10.1111/j.1365-2818.2008.02014.x

Piazolo, S., Montagnat, M., Grennerat, F., Moulinec, H., & Wheeler, J. (2015). Effect of local stress heterogeneities on dislocation fields. *Acta Materialia*, *90*, 303–309. https://doi.org/10.1016/j.actamat.2015.02.046

Piazolo, S., Wilson, C. J. L., Luzin, V., Brouzet, C., & Peternell, M. (2013). Dynamics of ice mass deformation: Linking processes to rheology, texture, and microstructure. *Geochemistry, Geophysics, Geosystems*, *14*(10), 4185–4194. https://doi.org/10.1002/ggge.20246

Pimienta, P., & Duval, P. (1987). Mechanical behavior of anisotropic polar ice. *The Physical Basis of Ice Sheet Modelling*, *170*, 57–66.

Placidi, L., Greve, R., Seddik, H., & Faria, S. H. (2010). Continuum-mechanical, Anisotropic Flow model for polar ice masses, based on an anisotropic Flow Enhancement factor. *Continuum Mechanics and Thermodynamics*, *22*(3), 221–237. https://doi.org/10.1007/s00161-009-0126-0

Prior-Jones, M. R., Bagshaw, E. A., Lees, J., Clare, L., Burrow, S., Werder, M. A., et al. (2021). Cryoegg: Development and field trials of a wireless subglacial probe for deep, fast-moving ice. *Journal of Glaciology*, *67*, 620–627. https://doi.org/10.1017/jog.2021.16

Qi, C., Prior, D. J., Craw, L., Fan, S., Llorens, M.-G., Griera, A., et al. (2019). Crystallographic preferred orientations of ice deformed in direct-shear experiments at low temperatures. *The Cryosphere*, *13*(1), 351–371. https://doi.org/10.5194/tc-13-351-2019

Ramsay, J. (1980). Shear zone geometry: A review. *Shear Zones in Rocks*, *2*(1), 83–99. https://doi.org/10.1016/0191-8141(80)90038-3

Rathmann, N. M., Hvidberg, C. S., Grinsted, A., Lilien, D. A., & Dahl-Jensen, D. (2021). Effect of an orientation-dependent non-linear grain fluidity on bulk directional enhancement factors. *Journal of Glaciology*, *67*(263), 569–575. https://doi.org/10.1017/jog.2020.117

Rathmann, N. M., & Lilien, D. A. (2021). Inferred basal friction and mass flux affected by crystal-orientation fabrics. *Journal of Glaciology*, *68*(268), 1–17. https://doi.org/10.1017/jog.2021.88

Richards, D. H. (2023). dhrichards/BridgingTheGapFigures: Revision release. [Software]. Zenodo. https://doi.org/10.5281/zenodo.10020144

Richards, D. H., Pegler, S. S., & Piazolo, S. (2022). Ice fabrics in two-dimensional flows: Beyond pure and simple shear. *The Cryosphere*, *16*(10), 4571–4592. https://doi.org/10.5194/tc-16-4571-2022

Richards, D. H., Pegler, S. S., Piazolo, S., & Harlen, O. G. (2021). The evolution of ice fabrics: A continuum modelling approach validated against laboratory experiments. *Earth and Planetary Science Letters*, *556*, 116718. https://doi.org/10.1016/j.epsl.2020.116718

Shepherd, A., Ivins, E., Rignot, E., Smith, B., van den Broeke, M., & Velicogna, I. (2018). The IMBIE team mass balance of the Antarctic ice sheet from 1992 to 2017. *Nature*, *558*(7709), 219–222. https://doi.org/10.1038/s41586-018-0179-y

Smith, E., Baird, A., Kendall, J., Martín, C., White, R., Brisbourne, A., & Smith, A. (2017). Ice fabric in an Antarctic ice stream interpreted from seismic anisotropy. *Geophysical Research Letters*, *44*, 3710–3718. https://doi.org/10.1002/2016GL072093

Stoll, N., Eichler, J., Hörhold, M., Erhardt, T., Jensen, C., & Weikusat, I. (2021). Microstructure, micro-inclusions, and mineralogy along the EGRIP ice core—Part 1: Localisation of inclusions and deformation patterns. *The Cryosphere*, *15*(12), 5717–5737. https://doi.org/10.5194/tc-15-5717-2021

Stoll, N., & Weikusat, I. (2023). C-axis data from 3 depths at EGRIP [Dataset]. Zenodo. https://doi.org/10.5281/zenodo.8015759

Svahnberg, H., & Piazolo, S. (2010). The initiation of strain localisation in plagioclase-rich rocks: Insights from detailed microstructural analyses. *Journal of Structural Geology*, *32*(10), 1404–1416. https://doi.org/10.1016/j.jsg.2010.06.011

Thomas, R. E., Negrini, M., Prior, D. J., Mulvaney, R., Still, H., Bowman, M. H., et al. (2021). Microstructure and crystallographic preferred orientations of an azimuthally oriented ice core from a lateral shear margin: Priestley glacier, Antarctica. *Frontiers in Earth Science*, *9*, 1084. https://doi.org/10.3389/feart.2021.702213

Thorsteinsson, T., Kipfstuhl, J., & Miller, H. (1997). Textures and fabrics in the GRIP ice core. *Journal of Geophysical Research*, *102*(C12), 26583–26599. https://doi.org/10.1029/97JC00161

Treverrow, A., Warner, R. C., Budd, W. F., & Craven, M. (2010). Meteoric and marine ice crystal orientation fabrics from the Amery Ice Shelf, East Antarctica. *Journal of Glaciology*, *56*(199), 877–890. https://doi.org/10.3189/002214310794457353

Vallelonga, P., Christianson, K., Alley, R. B., Anandakrishnan, S., Christian, J. E. M., Dahl-Jensen, D., et al. (2014). Initial results from geophysical surveys and shallow coring of the Northeast Greenland Ice Stream (NEGIS). *The Cryosphere*, *8*(4), 1275–1287. https://doi.org/10.5194/tc-8-1275-2014

Warren, J. M., & Hirth, G. (2006). Grain size sensitive deformation mechanisms in naturally deformed peridotites. *Earth and Planetary Science Letters*, *248*(1–2), 438–450. https://doi.org/10.1016/j.epsl.2006.06.006

Weikusat, I., Stoll, N., Kerch, J., Eichler, J., Jansen, D., & Kipfstuhl, S. (2022). Crystal c-axes (fabric analyser G50) of ice core samples (vertical thin sections) collected from the polar ice core EGRIP, 111–1714 m depth [Dataset]. PANGAEA. https://doi.org/10.1594/PANGAEA.949248

Westhoff, J., Stoll, N., Franke, S., Weikusat, I., Bons, P., Kerch, J., et al. (2021). A stratigraphy-based method for reconstructing ice core orientation. *Annals of Glaciology*, *62*(85–86), 191–202. https://doi.org/10.1017/aog.2020.76

Wilson, C. J. L., Peternell, M., Piazolo, S., & Luzin, V. (2014). Microstructure and fabric development in ice: Lessons learned from in situ experiments and implications for understanding rock evolution. *Journal of Structural Geology*, *61*, 50–77. https://doi.org/10.1016/j.jsg.2013.05.006

Wilson, C. J. L., Russell-Head, D. S., & Sim, H. M. (2003). The application of an automated fabric analyzer system to the textural evolution of folded ice layers in shear zones. *Annals of Glaciology*, *37*, 7–17. https://doi.org/10.3189/172756403781815401

Zeising, O., Gerber, T. A., Eisen, O., Ershadi, M. R., Stoll, N., Weikusat, I., & Humbert, A. (2023). Improved estimation of the bulk ice crystal fabric asymmetry from polarimetric phase co-registration. *The Cryosphere*, *17*(3), 1097–1105. https://doi.org/10.5194/tc-17-1097-2023

Zhang, Y., Hobbs, B. E., & Jessell, M. W. (1994). The effect of grain-boundary sliding on fabric development in polycrystalline aggregates. *Journal of Structural Geology*, *16*(9), 1315–1325. https://doi.org/10.1016/0191-8141(94)90072-8